Post-print of: P. Dworakowski, A. Wilk, M. Michna, B. Lefebvre and T. Lagier, "3-phase medium frequency transformer for a 100kW 1.2kV 20kHz Dual Active Bridge converter," IECON 2019 - 45th Annual Conference of the IEEE Industrial Electronics Society, Lisbon, Portugal, 2019, pp. 4071-4076, doi: 10.1109/IECON.2019.8926695.

3-phase medium frequency transformer for a 100kW 1.2kV 20kHz Dual Active Bridge converter

Piotr Dworakowski
SuperGrid Institute
Villeurbanne, France
piotr.dworakowski@supergrid-institute.com

Andrzej Wilk
Gdansk University of Technology
Faculty of Electrical and Control Engineering
Gdansk, Poland

Michal Michna
Gdansk University of Technology
Faculty of Electrical and Control Engineering
Gdansk, Poland

Bruno Lefebvre
SuperGrid Institute
Villeurbanne, France

Thomas Lagier
SuperGrid Institute
Villeurbanne, France

***Abstract*—The article presents a three-phase Medium Frequency Transformer being a part of a 100kW 1.2kV 20kHz Dual Active Bridge DC-DC converter. The transformer design is detailed focusing on winding and core power loss calculation. The high power three-phase MFT prototype is presented. The experimental results include the transformer impedance characteristics, no load test and three-phase DAB full load test waveforms.**

Keywords—Medium Frequency Transformer, power converter, DC-DC, Dual Active Bridge, Solid State Transformer

I. INTRODUCTION

The isolated DC-DC converter becomes the key technology in photovoltaic [1], wind energy [2], [3] and electric vehicle [4] applications or as a subsystem in Solid State Transformers for distribution grids [5] or railway traction [6] (Fig. 1).

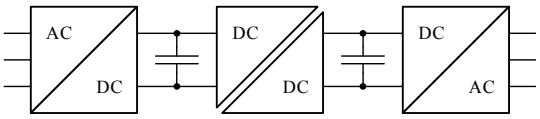

Fig. 1. Solid State Transformer diagram based on a 3 stage conversion with an isolated DC-DC converter

One of the most promising isolated DC-DC topologies for high power applications is the Dual Active Bridge (DAB) [7]. The series and/or parallel connection of elementary DABs allows to increase the voltage and power to build converters well suited for medium voltage and potentially extensible to high voltage applications [8]. On the other hand there is a well-developed family of non-isolated DC-DC topologies presented in [9] and [10].

The Medium Frequency Transformer (MFT) is one of the key components of the DAB. This is still quite a novel technology with lots of research interest. The selected designs of high power transformers operating at medium frequency are reported in: [11] at 100kW 10kHz, [12] at 400kW 5kHz and [13] at 1MW 20kHz. In [14] there is an interesting theoretical discussion on the MFT for HVDC applications.

This article presents a 3-phase MFT prototype being a part of a 100kW 1.2kV 20kHz DC-DC converter reported in [15]. The 3-phase DAB is described showing the requirements for the transformer. The 3-phase MFT design process is detailed resulting in a novel prototype. The experimental results prove the validity of the transformer design and highlight the remaining challenges.

II. DUAL ACTIVE BRIDGE DC-DC CONVERTER

A. 3-phase DAB motivation

The 3-phase DAB offers several advantages over the single-phase DAB:

- the DC capacitor size can be significantly reduced thanks to the $2\pi/3$ phase shift in the voltage ripple,
- for a given rating of the power semiconductor switch the converter power is higher thanks to natural current paralleling,
- the turn off current of the power semiconductor switch is lower,
- the magnetic circuit of the transformer is more compact,
- the voltage and current harmonics are lower resulting in lower transformer power loss,
- the transformer vector group can be chosen to optimize the converter design.

According to the authors' knowledge, only one 3-phase MFT prototype has been reported in [17] at 10kVA 1kHz. A 5MW 3-phase DAB was presented in [18] but using three single-phase MFTs. No 3-phase MFT at high power and high frequency has been reported.

B. 3-phase DAB operation

The 3-phase DAB is composed of two 3-phase Voltage Source Converters (VSC) connected with a 3-phase transformer as presented in Fig. 2.

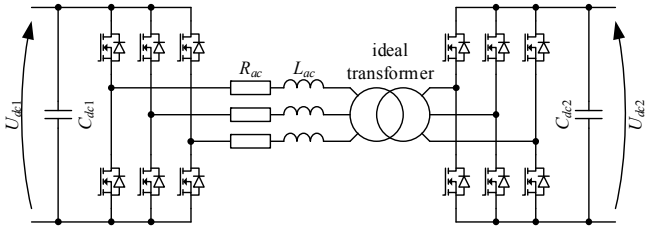

Fig. 2. 3-phase Dual Active Bridge circuit diagram

The transformer is modelled with the resistance R_{ac}, the inductance L_{ac} and the ideal transformer. The transformer vector group Yy is detailed in Fig. 3.

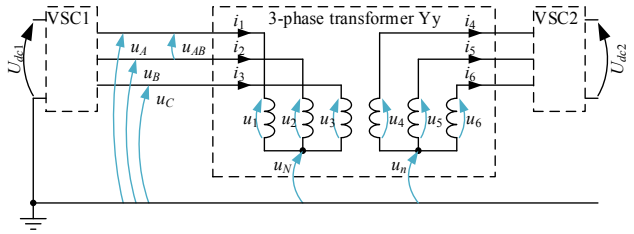

Fig. 3. Voltages and currents of the 3-phase Dual Active Bridge with Yy transformer

In DAB converters each VSC generates a square waveform. It has a controlled duty cycle and a controlled phase shift δ between the voltages of the corresponding phase of both VSCs. The rectangular modulation was selected which assumes the 50% duty cycle and the only controlled variable is the phase shift δ. The idealized waveforms of the 3-phase VSC are presented in Fig. 4.

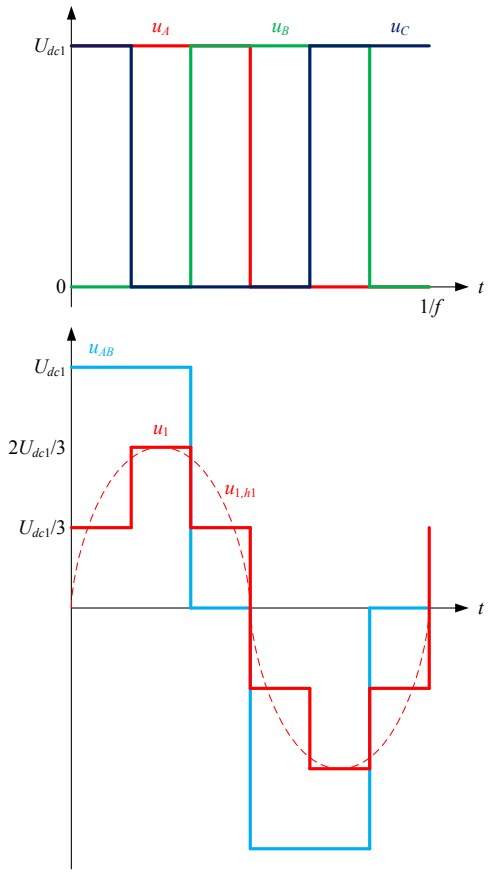

Fig. 4. Idealized voltage waveforms of the 3-phase VSC and transformer

In order to simplify the circuit analysis, a fundamental model at switching frequency f and neglecting the resistance R_{ac} is considered [7]. The balanced 3-phase voltages are assumed. The fundamental $u_{i,h1}$ of the voltage u_i where i=1...6 is calculated using the Fourier transform. The RMS value of the primary voltage fundamental is defined as U_{ac1} and the secondary as U_{ac2}. They are calculated according to (1) and (2) respectively. A basic circuit analysis leads to the active and reactive power formulation as defined in (3) and (4) respectively. The apparent power is defined in (5).

$$U_{ac1} = \frac{\sqrt{2}}{\pi} U_{dc1} \tag{1}$$

$$U_{ac2} = \frac{\sqrt{2}}{\pi} U_{dc2} \tag{2}$$

$$P_{ac} = 3 \frac{U_{ac1} U_{ac2}}{2\pi f L_{ac}} \sin\delta \tag{3}$$

$$Q_{ac} = 3 \frac{U_{ac1}}{2\pi f L_{ac}} (U_{ac1} - U_{ac2} \cos\delta) \tag{4}$$

$$S_n = \sqrt{{P_{ac}}^2 + {Q_{ac}}^2} \tag{5}$$

C. DC-DC converter prototype

A DAB converter prototype was developed and reported in [15]. The converter specification is presented in TABLE I. The converter is based on SiC MOSFET which enables the high frequency operation and 20kHz was found to be a good compromise between the switching loss and passive component size. The discussion on the power electronics switching is presented in [16]. The converter was designed to operate in single-phase and 3-phase configurations. It was first equipped with a single-phase MFT and successfully tested.

TABLE I. DC-DC CONVERTER PROTOTYPE SPECIFICATION

Parameter	Value
Nominal power	100kW
Nominal input DC voltage	1200V
Minimum input DC voltage	900V
Nominal step-down ratio	1 or 0.5
Maximum converter step-down ratio variation	±10%
Nominal efficiency	98%
Cooling	Forced air

III. 3-PHASE MEDIUM FREQUENCY TRANSFORMER DESIGN

A. Design constraints

In order to perform the comparative analysis between the single-phase and the 3-phase MFT, it was decided to use the same core material MnZn ferrite 3C90 from Ferroxcube. Since the C-cores and E-cores do not exist for such big transformers then the I-cores had to be used. With the single-phase MFT, it was observed quite a high winding capacitance causing important undesirable voltage oscillations [19]. For the 3-phase MFT, it was decided to avoid the foil winding and to use a litz wire winding. The transformer ratio was set to 1:1 and the vector group was set to Yy as it results in smaller MFT size. The leakage inductance requirement was set to as low as possible in order to reduce the power electronics loss but higher than 15µH due to converter control constraints.

B. Preliminary design

According to the requirements of the DC-DC converter prototype and the design constraints, a set of design inputs was defined as presented in TABLE II.

TABLE II. 3-PHASE MFT DESIGN INPUTS

Parameter	Value
Maximum operating frequency	23kHz
Minimum operating frequency	17kHz
Maximum winding current density	3A/mm^2
Maximum core flux density	0.3T

The transformer design methodology for power electronics applications is described in [20] and it is well documented in the scientific literature. Based on those a transformer specification can be defined as presented in TABLE III. The transformer dimensions presented in Fig. 5 were set to meet the manufacturing constraints and the required leakage inductance according to [21]. This specification is used for the detailed winding and core design presented in the following sections.

TABLE III. 3-PHASE MFT SPECIFICATION

Parameter	Value
Nominal apparent power	150kVA
Winding turn number	20
Core cross-section	12.5cm^2

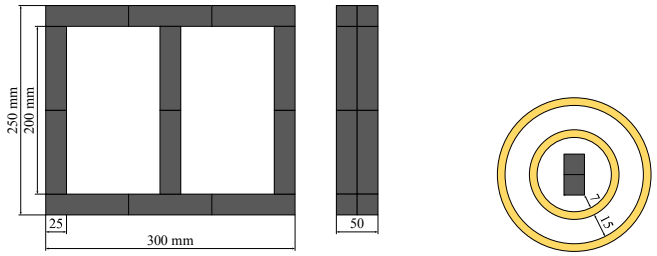

(a) (b)

Fig. 5. 3-phase MFT dimensions: core (a), winding (b)

C. *Winding detailed design*

The DC resistance of the transformer winding R_{dc} can be simply calculated based on dimensions. However, the AC resistance R_{ac} is far more complex to calculate due to skin and proximity effects. The analytical equation of the AC resistance for foil winding was proposed by Dowell in [22]. In this article, the method for round litz wire from [23] was used. The AC resistance of the litz wire is defined in (6)

$$R_{ac} = K_d R_{dc} \tag{6}$$

where K_d is a function of frequency, wire conductivity, wire diameter, number of strands, packing factor and number of winding layers. Obviously, the best performance is obtained for the thinnest strand but due to mechanical constraints, the strand diameter is limited to 0.1mm for large wires. Eventually, the litz wire defined in TABLE IV was chosen. The single layer winding was selected. The round winding was required due to the high bending radius of the litz wire.

TABLE IV. LITZ WIRE SPECIFICATION

Parameter	Value
Strand diameter	0.1mm
Number of strands in the wire	3870
Nominal wire cross section	30.39mm^2
Packing factor	0.56

The evaluation of R_{ac} requires a harmonic decomposition of the winding current in order to calculate the K_d for each harmonic. The idealized voltage and current waveforms are presented in Fig. 6 and Fig. 7 for nominal and degraded mode respectively. The corresponding harmonic decomposition is presented in Fig. 8. It can be observed a higher current in the degraded mode but the current harmonic distortion is higher in the nominal mode. The nominal mode is characterized by $U_{dc2} = U_{dc1}$ and the degraded mode by $U_{dc2} = 0.8U_{dc1}$.

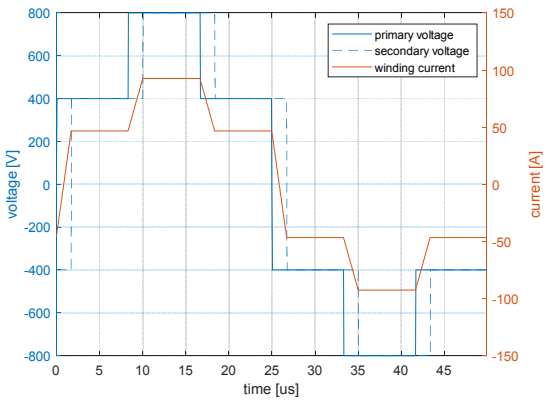

Fig. 6. Idealized voltage and current waveforms for the nominal mode at U_{dc1} = 1200V and 100kW

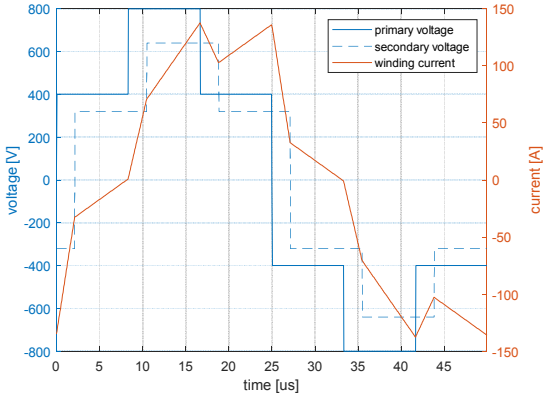

Fig. 7. Idealized voltage and current waveforms for the degraded mode at U_{dc1} = 1200V and 100kW

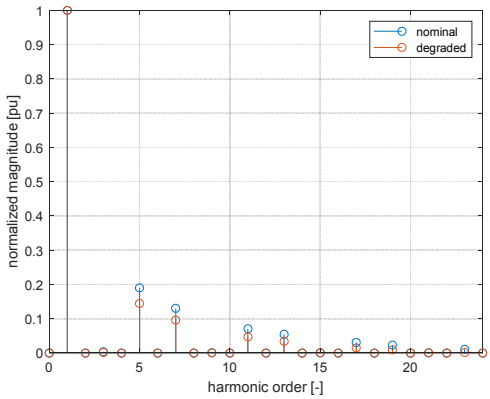

Fig. 8. Current harmonics normalized to fundamental for the nominal and degraded mode

Finally, the winding specification is presented in TABLE V. The equivalent series resistance is higher in the nominal mode due to higher harmonic distortion. However, the winding RMS current is higher in the degraded mode. Overall the winding power loss is higher in the degraded mode so this should be considered in the thermal design.

TABLE V. WINDING SPECIFICATION AT 80°C

Parameter	Nominal mode	Degraded mode
Equivalent series resistance R_{ac}	17.1mΩ	14.4mΩ
Winding RMS current I_{RMS}	64A	92A
Winding power loss P_w	214W	365W

D. Core detailed design

The analytical equation of core power loss for sinusoidal excitation was proposed by Steinmetz in [24]. An extended formula taking into account the core temperature is defined in (7) and (8) based on [25]

$$P_{c\,sin} = k f^{\alpha} {B_{max}}^{\beta} k_T V_c \tag{7}$$

$$k_T = c_0 - c_1 T + c_2 T^2 \tag{8}$$

where f is the frequency, B_{max} is the maximum flux density, V_c is the core volume, T is the core temperature, c_x is the temperature coefficient and k, α, β are the Steinmetz coefficients presented in TABLE VI.

In [26] it was proposed a modification of the power loss formula for non-sinusoidal excitations but still using the Steinmetz coefficients only. The core power loss is defined in (9)

$$P_c = k_s k_T V_c (2B_{max})^{\beta-\alpha} \frac{1}{T} \int_0^T \left| \frac{u_i}{N_1 A_c} \right|^{\alpha} dt \tag{9}$$

where u_i is the i-th winding voltage (i=1...6), $T = f^{-1}$, N_1 is the number of primary turns, A_c is the core cross-section and k_s is defined in (10).

$$k_s = \frac{k}{2^{\beta+1}\pi^{\alpha-1}\left(0.2761 + \frac{1.7061}{\alpha + 1.354}\right)} \tag{10}$$

TABLE VI. FERRITE 3C90 STEINMETZ COEFFICIENTS [25]

Parameter	Value
k	3.2
α	1.46
β	2.75
c_0	2.45
c_1	3.1e-2
c_2	1.65e-4

The evaluation of core loss requires knowledge on the voltage and flux density waveforms. The idealized flux density waveform can be plotted as presented in Fig. 9.

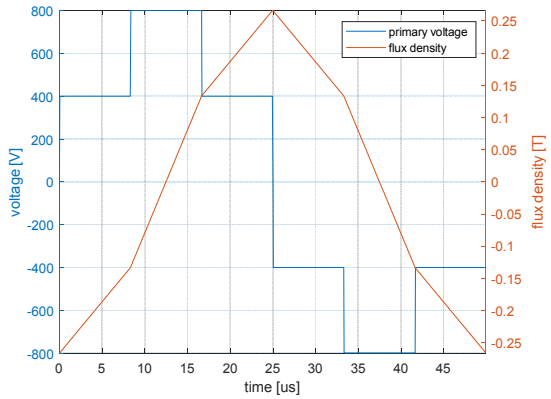

Fig. 9. Idealized voltage and flux density waveforms at U_{dc1} = 1200V

Finally, the core specification is presented in TABLE VII. The calculated core loss has a similar value to the winding loss at the nominal operation in order to maximize the efficiency. It is lower than the winding loss in the degraded mode in order to ensure the efficient transformer cooling.

TABLE VII. CORE SPECIFICATION AT 100°C

Parameter	Value
Core flux density B_{max}	0.27T
Core power loss P_c	230W

Based on the detailed design outputs a finite element verification was performed. Thermal performance was simulated allowing to check the winding and core temperature. The mechanical design was done prior to the 3-phase MFT manufacturing.

IV. EXPERIMENTAL VERIFICATION

A. Experimental setup

A dedicated power converter test bench was developed allowing the experimental validation of the 3-phase DAB. The circuit diagram is presented in Fig. 10 and the test bench implementation in Fig. 11. The power circuit is arranged in back-to-back in order to test the DC-DC converter at full power with minimum energy consumption. The converter output is connected to its input and the whole is supplied from the DC power supply which sets the voltage reference and supplies the test circuit power loss. If the DC-DC step-down ratio is different from 1 then two DC-DC converters are required. The DC inductors are used to decouple the VSCs. The DC-DC converter operates in the power regulation mode using the DC voltage and DC current transducers. The current transducers in the AC link are necessary for the internal converter protection. They may be also used for the control of the transformer DC current.

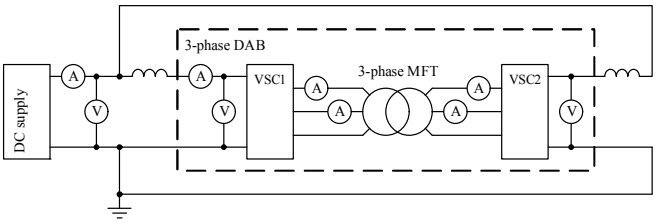

Fig. 10. 3-phase DAB test bench diagram

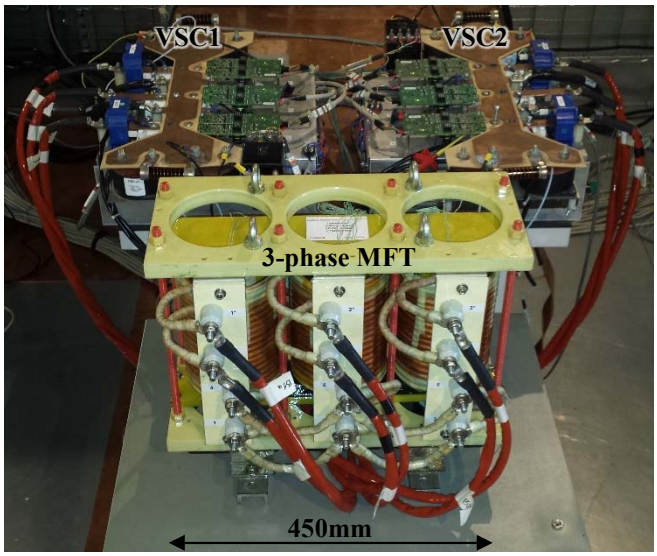

Fig. 11. 3-phase DAB test bench implementation

B. *Experimental results*

The winding resistance and the leakage inductance were measured using the impedance analyzer Wayne Kerr 6500B. The measurement was performed on the primary winding with the corresponding secondary in short circuit in order to achieve the magnetic flux compensation. The comparison of calculated and measured winding resistance in the function of frequency is presented in Fig. 12. It shows quite a good fit over the entire frequency range. The small difference can be explained by some inaccuracies in winding dimensions.

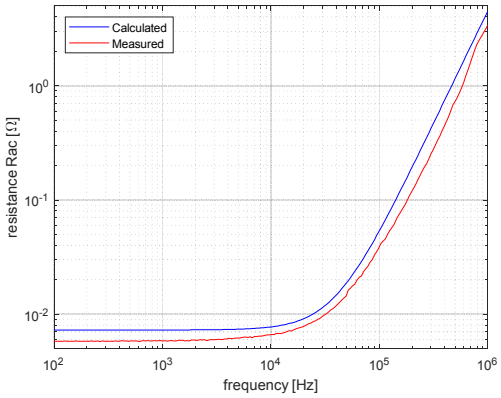

Fig. 12. Winding resistance in the function of frequency at 20°C

In Fig. 13 there is presented the transformer no-load test result. The VSC1 operates normally at U_{dc1} = 1200V and the AC terminals of the VSC2 are disconnected. The waveforms show the transformer primary winding voltage measured at transformer terminals and the primary winding current. The voltage waveforms present some oscillations due to transformer parasitic capacitance and connection wire inductance. As expected the magnetizing current in phase B is lower than in phase A and C due to natural dissymmetry in the magnetic core. The current in phase A is slightly lower than in phase C probably due to core assembly imperfections. The magnetizing inductance was calculated based on the measured waveforms.

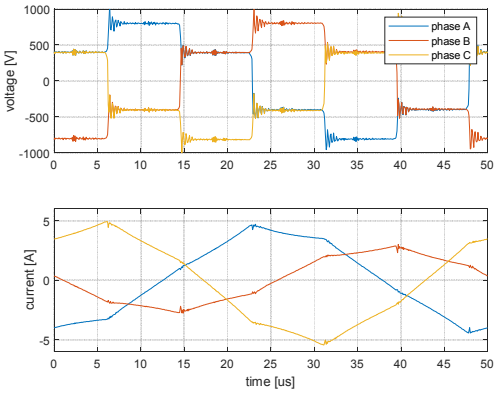

Fig. 13. 3-phase MFT no load test waveforms at U_{dc1} = 1200V

The comparison synthesis of average winding resistance and inductance is presented in TABLE VIII. The measured winding resistance is lower than calculated probably due to simplified calculations and inaccurate winding dimensions. It shall be noted that the presented winding resistance at 20kHz is different from the equivalent series resistance R_{ac}. The R_{ac} takes into account all current harmonics resulting from the DAB operation and it cannot be measured directly. The leakage inductance shows a good fit but the magnetizing inductance is lower than expected from calculations. This is probably due to multiple air gaps in the core which were not taken into account in the design. The magnetizing inductance and the core power loss need to be further analyzed according to investigations proposed in [27].

TABLE VIII. COMPARISON OF CALCULATED AND MEASURED AVERAGE RESISTANCE AND INDUCTANCE AT 20KHZ AND 20°C

Parameter	Calculated	Measured
Winding resistance	9.1mΩ	7.8mΩ
Leakage inductance	14.9μH	15.8μH
Magnetizing inductance	6.5mH	1.8mH

In Fig. 14 there is presented the 3-phase DAB full load test result at 100kW. In this test both VSC1 and VSC2 operate at $U_{dc2} \approx U_{dc1}$ = 1200V with δ regulated to achieve the required power flow. The waveforms show the VSC1 and VSC2 voltage measured at inverter terminals and the VSC1 current. The inverter terminal voltage has less oscillations than the transformer terminal voltage (Fig. 13) due to the connection wire inductance. The measured waveforms can be compared to the idealized waveforms from Fig. 6. A good fit is observed. In Fig. 15 there is presented a similar test result but at $U_{dc2} \approx U_{dc1}$ = 900V. The converter operation is still correct. The only difference is the higher current. The degraded mode operation was not tested due to the test bench limitation requiring $U_{dc2} \approx U_{dc1}$. The DC voltage ripple was too low to be measured precisely.

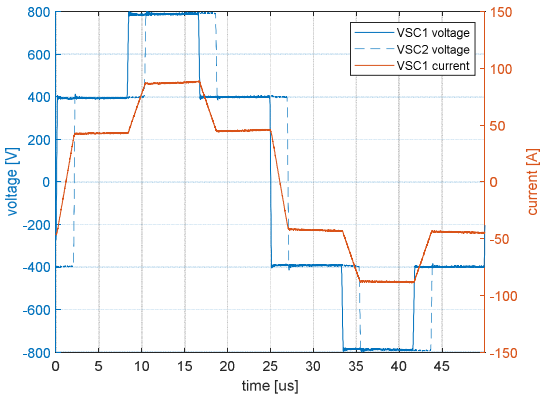

Fig. 14. 3-phase DAB full load test waveforms phase A at U_{dc1} = 1200V and 100kW

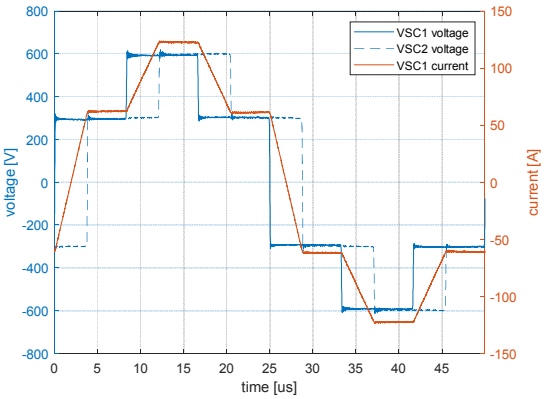

Fig. 15. 3-phase DAB full load test waveforms phase A at U_{dc1} = 900V and 100kW

V. Conclusion

The 3-phase Medium Frequency Transformer has been presented together with the 100kW 1.2kV 20kHz Dual Active Bridge DC-DC converter. The transformer design was detailed giving the specifications of the winding and core. The 3-phase MFT prototype was shown and tested at no load and full power.

This article presents the feasibility of a high power 3-phase MFT. The design methods commonly used for single-phase transformers seem valid for 3-phase devices. Some of the 3-phase DAB motivations were demonstrated. The DC voltage ripple was observed very low making the precise measurement challenging. The AC current was measured lower than in the single-phase DAB. The transformer voltage and current harmonic content was lower what shall result in higher transformer efficiency.

The main difficulty of the 3-phase MFT is the mechanical design of the ferrite core ensuring a controlled air gap for the controlled value of magnetizing inductance. Overall the electromagnetic interference remains one of the main challenges of the SiC-based power converters.

The authors will focus on the power loss measurements of the VSC and the transformer as well as on the verification of the thermal design. The influence of the 3-phase transformer vector group will be further analyzed.

Acknowledgment

This work was supported by a grant overseen by the French National Research Agency (ANR) as part of the "Investissements d'Avenir" Program (ANE-ITE-002-01).

References

[1] G. R. Walker and P. C. Sernia, "Cascaded DC-DC converter connection of photovoltaic modules," IEEE Transactions on Power Electronics, vol. 19, no. 4, pp. 1130–1139, Jul. 2004

[2] M. D. P. Gil, J. L. Domínguez-García, F. Díaz-González, M. Argues-Peñalba, and O. Gomis-Bellmunt, "Feasibility analysis of offshore wind power plants with DC collection grid," Renewable Energy, vol. 78, pp. 467–477, 2015

[3] C. G. Dincan et al., "Design of a High-Power Resonant Converter for DC Wind Turbines," in IEEE Transactions on Power Electronics, vol. 34, no. 7, pp. 6136-6154, July 2019

[4] Y. Du, S. Lukic, B. Jacobson, and A. Huang, "Review of high power isolated bi-directional DC-DC converters for PHEV/EV DC charging infrastructure," 2011 IEEE Energy Conversion Congress and Exposition, pp. 553–560, 2011

[5] X. She, A. Q. Huang and R. Burgos, "Review of Solid-State Transformer Technologies and Their Application in Power Distribution Systems," in IEEE Journal of Emerging and Selected Topics in Power Electronics, vol. 1, no. 3, pp. 186-198, Sept. 2013

[6] C. Stackler, F. Morel, P. Ladoux, A. Fouineau, F. Wallart and N. Evans, "Optimal sizing of a power electronic traction transformer for railway applications," IECON 2018 - 44th Annual Conference of the IEEE Industrial Electronics Society, Washington, DC, 2018, pp. 1380-1387

[7] R. W. A. A. De Doncker, D. M. Divan and M. H. Kheraluwala, "A three-phase soft-switched high-power-density DC/DC converter for high-power applications," in IEEE Transactions on Industry Applications, vol. 27, no. 1, pp. 63-73, Jan.-Feb. 1991

[8] J. D. Páez, D. Frey, J. Maneiro, S. Bacha and P. Dworakowski, "Overview of DC–DC Converters Dedicated to HVdc Grids," in IEEE Transactions on Power Delivery, vol. 34, no. 1, pp. 119-128, Feb. 2019

[9] D. Jovcic and L. Zhang, "LCL DC/DC Converter for DC Grids," in IEEE Transactions on Power Delivery, vol. 28, no. 4, pp. 2071-2079, Oct. 2013

[10] M. S. Bhaskar, S. Padmanaban, V. Fedák, F. Blaabjerg, P. W. Wheeler and V. K. Ramachandaramurthy, "L-L multilevel boost converter topology for renewable energy applications: A new series voltage multiplier L-L converter of XY family," 2017 19th International Conference on Electrical Drives and Power Electronics (EDPE), Dubrovnik, 2017, pp. 133-138

[11] M. Mogorovic and D. Dujic, "100 kW, 10 kHz Medium-Frequency Transformer Design Optimization and Experimental Verification," in IEEE Transactions on Power Electronics, vol. 34, no. 2, pp. 1696-1708, Feb. 2019

[12] I. Villar, L. Mir, I. Etxeberria-Otadui, J. Colmenero, X. Agirre and T. Nieva, "Optimal design and experimental validation of a Medium-Frequency 400kVA power transformer for railway traction applications," 2012 IEEE Energy Conversion Congress and Exposition (ECCE), Raleigh, NC, 2012, pp. 684-690

[13] G. Ortiz, J. Biela, D. Bortis and J. W. Kolar, "1 Megawatt, 20 kHz, isolated, bidirectional 12kV to 1.2kV DC-DC converter for renewable energy applications," The 2010 International Power Electronics Conference - ECCE ASIA -, Sapporo, 2010, pp. 3212-3219

[14] T. Lüth, M. M. C. Merlin, T. C. Green, F. Hassan and C. D. Barker, "High-Frequency Operation of a DC/AC/DC System for HVDC Applications," in IEEE Transactions on Power Electronics, vol. 29, no. 8, pp. 4107-4115, Aug. 2014

[15] T. Lagier et al., "A 100 kW 1.2 kV 20 kHz DC-DC converter prototype based on the Dual Active Bridge topology," 2018 IEEE International Conference on Industrial Technology (ICIT), Lyon, 2018, pp. 559-564

[16] T. Lagier and P. Ladoux, "Theoretical and experimental analysis of the soft switching process for SiC MOSFETs based Dual Active Bridge converters," 2018 International Symposium on Power Electronics, Electrical Drives, Automation and Motion (SPEEDAM), Amalfi, 2018, pp. 262-267

[17] Y. Lee, G. Vakil, A. J. Watson and P. W. Wheeler, "Geometry optimization and characterization of three-phase medium frequency transformer for 10kVA Isolated DC-DC converter," 2017 IEEE Energy Conversion Congress and Exposition (ECCE), Cincinnati, OH, 2017, pp. 511-518

[18] N. Soltau, H. Stagge, R. W. De Doncker and O. Apeldoorn, "Development and demonstration of a medium-voltage high-power DC-DC converter for DC distribution systems," 2014 IEEE 5th International Symposium on Power Electronics for Distributed Generation Systems (PEDG), Galway, 2014, pp. 1-8

[19] P. Dworakowski, A. Wilk and B. Lefebvre, "Hysteresis modelling of a medium frequency single-phase transformer," 2017 19th European Conference on Power Electronics and Applications (EPE'17 ECCE Europe), Warsaw, 2017, pp. P.1-P.9

[20] W.G. Hurley, W.H. Wölfle, "Transformers and Inductors for Power Electronics: Theory, Design and Applications," John Wiley & Sons, 2013

[21] A. Fouineau, M. Raulet, B. Lefebvre, N. Burais and F. Sixdenier, "Semi-Analytical Methods for Calculation of Leakage Inductance and Frequency-Dependent Resistance of Windings in Transformers," in IEEE Transactions on Magnetics, vol. 54, no. 10, pp. 1-10, Oct. 2018, Art no. 8400510

[22] P. L. Dowell, "Effects of eddy currents in transformer windings," in Proceedings of the Institution of Electrical Engineers, vol. 113, no. 8, pp. 1387-1394, August 1966

[23] F. Tourkhani and P. Viarouge, "Accurate analytical model of winding losses in round Litz wire windings," in IEEE Transactions on Magnetics, vol. 37, no. 1, pp. 538-543, Jan 2001

[24] C. P. Steinmetz, "On the Law of Hysteresis," in Transactions of the American Institute of Electrical Engineers, vol. IX, no. 1, pp. 1-64, Jan. 1892

[25] Ferroxcube, "Design of planar power transformers, application note," http://ferroxcube.home.pl/appl/info/plandesi.pdf

[26] K. Venkatachalam, C. R. Sullivan, T. Abdallah and H. Tacca, "Accurate prediction of ferrite core loss with nonsinusoidal waveforms using only Steinmetz parameters," 2002 IEEE Workshop on Computers in Power Electronics, 2002. Proceedings., Mayaguez, Puerto Rico, USA, 2002, pp. 36-41

[27] A. Wilk, M. Michna, P. Dworakowski and B. Lefebvre, "Influence of air gap size on magnetizing current and power losses in ferrite core transformers - experimental investigations," Twenty-fifth Symposium on Electromagnetic Phenomena in Nonlinear Circuits (EPNC), Arras, 2018